Supplementary Information

Bottom-up Direct Write Approach to Controlled Fabrication of WS_2/MoS_2 Heterostructure Systems

Rui Dong,[a] Logan Moore,[a] Nozima Aripova,[b] Christopher Williamson,[a] Robert Schurz,[a] Yuzi Liu[c], Leonidas E. Ocola,[c] and Irma Kuljanishvili[a]*

[a]Department of Physics, Saint Louis University, St. Louis, MO, 63103, USA

[b]Department of Biology, Saint Louis University, St. Louis, MO, 63103, USA

[c]Argonne National Laboratory, 9700 S. Cass Avenue, Argonne, IL, 60439, USA

*Email: ikuljani@slu.edu

1. Two-step automated direct-write patterning.

The direct write patterning technique employed in this study consists of two main steps, i.e. the "inking" and "writing", which can be symbolically described as two steps imitating the handwriting on a paper using a pen or a quill. In the direct writing technique the AFM cantilever tips are used as pens. When multi-pen cantilevers are utilized, this allows for parallel writing so that large size arrays of patterns can be obtained with high throughput and efficiency. In the process of inking, the tip of an atomic force microscope (AFM) is dipped into the ink. Fig. S1a, shows the optical image of the inking step. Here, 12 pen cantilevers and corresponding number of ink reservoir channels, which have a matching pitch to the cantilever tip spacing, can be seen. In the writing step, the selected inks are transferred onto the substrate. Fig. S1b, shows the optical image representing the initial moment of the writing; here tips are shown in contact with the SiO_2/Si substrate. With the assistance of pre-patterned alphabetical markers on the substrates, which are used for alignment and location registry, the inks can be deposited on the selected area of the substrate by utilizing the high precision of the piezo-driven motorized stages. Pre-patterned alphabetical markers are made from Pt/Ti metal, (70nm/5nm, respectively), via standard e-beam lithography and lift-off process. Substrates then undergo extensive cleaning to remove possible leftover polymer residuals as described in the Experimental Section.

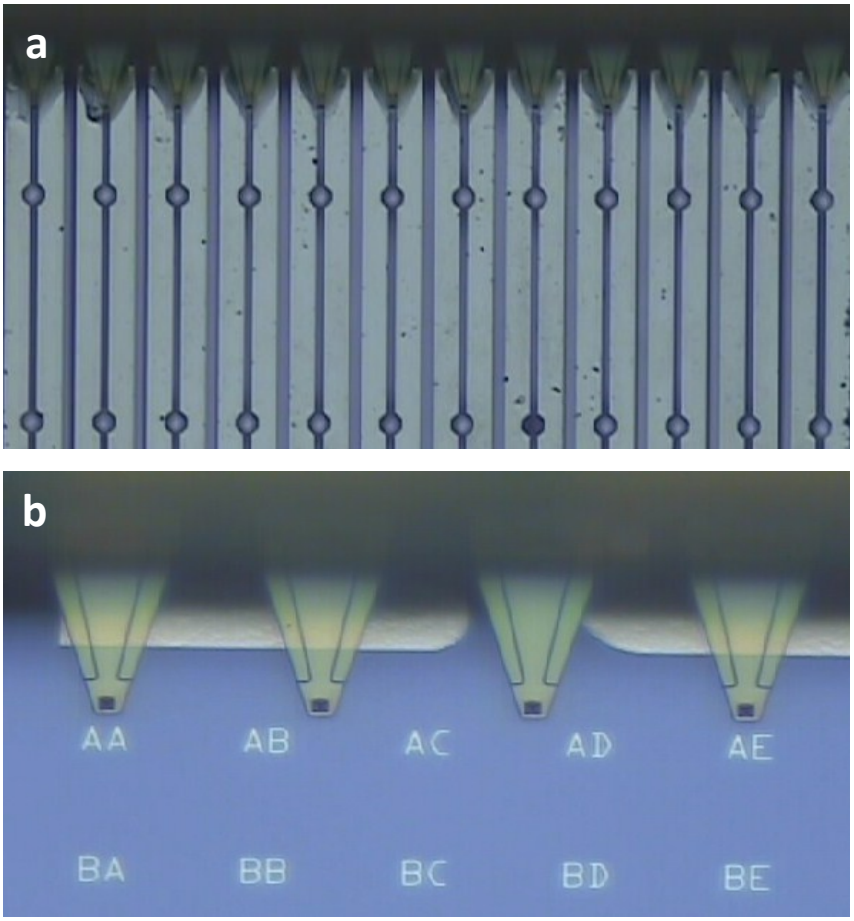

Fig. S1 The schematic view of the patterning process describing two main steps: a) Step 1, the "inking" process as denoted in the optical view where 12 tips are shown in the picture dipped into individual ink channels; b) Step 2, the "writing" process as denoted in optical view where a selected area is indicated with pre-patterned alphabetical markers and electrodes, (only 4 pens are shown touching the surface in the picture, the distance between numerical markers is approximately 55 μm).

2. Dot array patterns and other line shapes of fabricated MX_2.

With the direct write fabrication approach, complex structures can be potentially prepared with the combination of fabricated arrays of dot and ribbon structures using the software protocol sequencing. Arrays of dots are generally produced by holding the inked cantilever in contact with the substrate to establish the ink transfer from the tips to the substrate which is governed by the diffusion process. This way circular dot (ink droplets) patterns are generated. Then tip retracts and moves to the next position and the process is repeated. By optimizing parameters such as environmental humidity and temperature in the writing chamber, tip moving speed, dwell time and ink concentration the diameter and thickness of MX_2 dots can be controlled. Fig. S2a shows an example of 3x3 dot array of WS_2 structures on SiO_2/Si substrate. The lateral diameter of WS_2 dots can be controlled to achieve the sub-micrometer range. Structures that are shown in

the Fig. S2a are approximately 700 nm in diameter, although, thinner and smaller diameter structures could also be realized. The WS_2 dot array (3x3) shows uniform height of ~ 60 nm of each dot as depicted in the AFM height profile measurement (Fig. S2c). Larger ribbons, such as the L-shaped structure shown in AFM topography image (Fig. 2b) with the line profile can also be made easily. Fig. S2d shows approximately 100 nm thick structure with lateral size (line width) of approximately 6 µm. These examples demonstrate that thickness and lateral size of patterned structures can be controlled to easily fit specific applications.

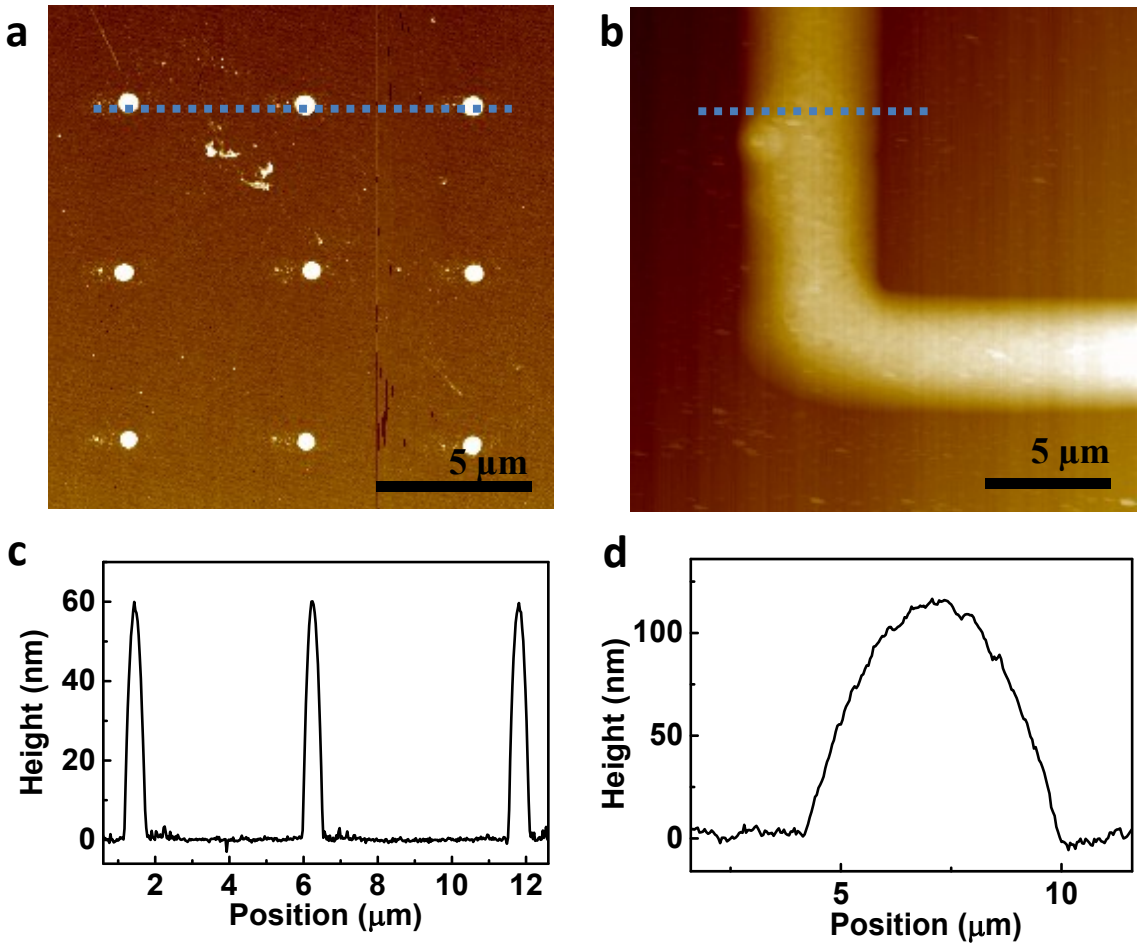

Fig. S2 Examples of WS_2 dots structures and L-shaped ribbon patterned on SiO_2/Si substrate: a) AFM topography image of the WS_2 dots array (3x3) and b) AFM topography image of L-shaped WS_2 structure. Line profiles shown in c) and d) represent AFM height measurements of the selected locations marked by a dotted line in AFM images in a) and b) respectively. WS_2 dot height and L-shaped ribbon height are approximately 60 nm and 110 nm respectively.

3. Patterns of WS_2/MoS_2 Heterostructures.

Flexibility of our direct writing approach allows for a convenient way to create a variety of architectures, assembled in different configurations. Fig.S3 shows a simple cross bar arrangement of two materials patterned in a two-step process. In the first step, parallel ribbons are written in x-axis directions with $(NH_4)_2MoS_4$ precursor ink and followed by the thermal annealing, as described in the Experimental Section, and in the second step $(NH_4)_2WS_4$ precursor ink is pattered in perpendicular direction (atop of MoS_2 ribbons) and also followed by another annealing process to finally form WS_2/MoS_2 heterostructures. AFM topography image (Fig. S3a) and corresponding height profiles of MoS_2, WS_2 ribbons and WS_2/MoS_2 cross bar area are shown in Fig. S3b, Fig. S3c and Fig. S3d, respectively. Regions where two materials are formed on top of each other represent cross-bar regions.

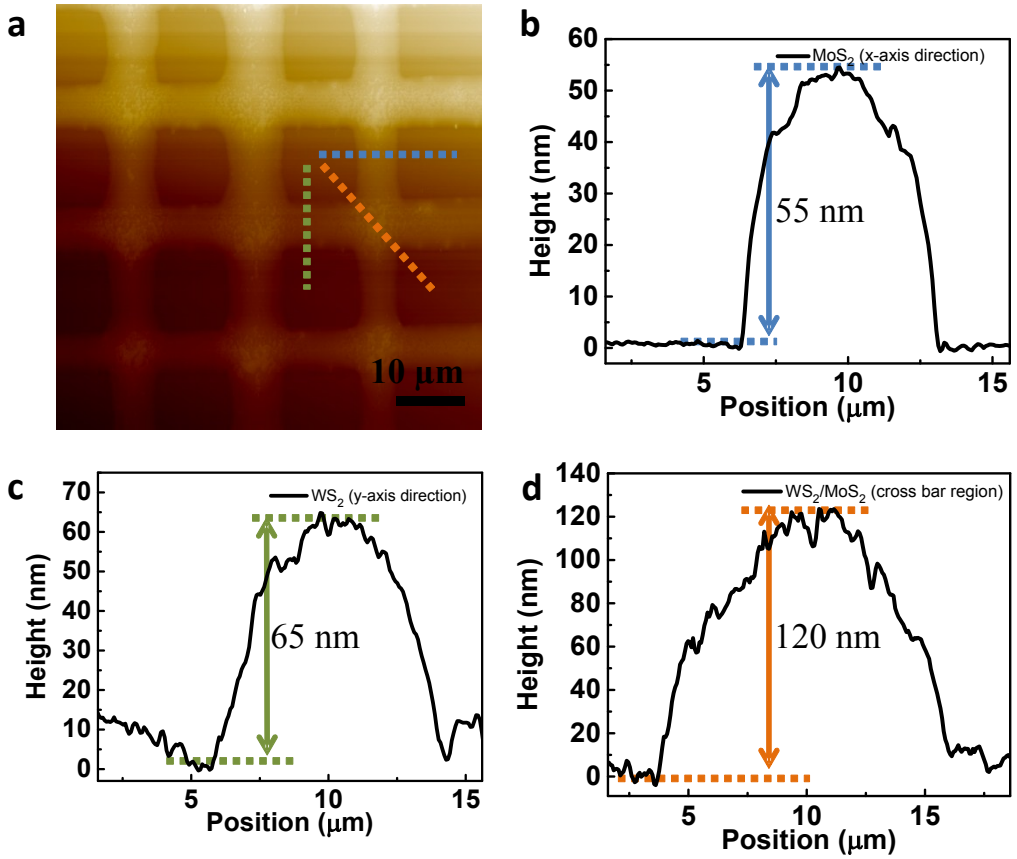

Fig. S3 AFM topography image of WS_2/MoS_2 heterostructure cross bars (3x3) and corresponding line profiles; a) AFM topography image of WS_2/MoS_2 heterostructure formed on SiO_2/Si, three dotted lines mark locations of height line profiles, b) Line profile of MoS_2 ribbon patterned in x-axis direction , c) Line profile of WS_2 ribbon patterned in y-axis direction, d) Line profile of the heterostructure cross-bar region. Height measurement in d) indicates the combined thickness of two materials at the cross bar region.

It must be noted that in ribbon writing, (Fig.S2b and Fig. S3a) tips are in continuous dynamic interaction with the substrate surface. Because liquid inks were employed in this study, we see the "dome shaped" profiles in the cross-sectional line scans (Fig. S3b-d). These shapes are often ascribed to the influence of liquid ink transfer dynamics[1-3]. In this particular example, we intentionally had relatively larger ink loading on the tips which was needed for continuous writing of long micrometer patterns. Here we operated in the regime of relatively fast ink transfer from the tip to the substrate. Substrate surface properties such as hydrophillicity or hydrophobicity could be adjusted to render thinner deposits by influencing the energy dynamics between substrate-ink and ink-intermolecular interactions. Additionally, one can potentially employ alternative solvents, such as carrier inks, for delivering the active ingredients, so that the ink transfer and diffusion dynamics can be further tuned to form flatter structures. In the present work, our choice of using wafer based inks was made because water is a chemically neutral and residue free solvent.

4. Patterns of $MoS_2/WS_2/MoS_2$ tri-layers structures.

More complicated heterostructures such as $MoS_2/WS_2/MoS_2$ tri-layer assemblies can also be easily obtained with the direct writing technique. Lateral heterostructures can be formed as easily as vertical heterostructures geometries, owing to the precision of scanning probe nanolithography based approach, such as the present technique. This method provides a simple and convenient route for creating complex structures.

The fabrication of tri-layer heterostructures is based on controlled writing of MX_2 ribbons in a repeated fashion with subsequent steps of crystallization performed after each patterning step to form final tri-layer architectures. As in earlier examples $(NH_4)_2MoS_4$ and $(NH_4)_2WS_4$ precursor inks were used. The step by step process is described below.

To fabricate vertically assembled tri-layer heterostructure, first we pattern a ribbon of $(NH_4)_2MoS_4$ precursor in horizontal direction (x-axis) for a desired length. We follow this step with the annealing of the sample in the CVD furnace to crystallize the precursor to form MoS_2 material. Then the sample is placed back into the patterning chamber, aligned with the aid of alphabetical alignment marks and then the diagonal ribbon of $(NH_4)_2WS_4$ precursor is patterned for a desired length. This pattern structure is made in such a way that it overlaps the MoS_2 patterned structure. We follow this step with annealing of the sample again in order to crystallize the $(NH_4)_2WS_4$ precursor to form WS_2 material. Then, once again, the sample is placed back into the patterning chamber, aligned to the pre-existing pattern, and then, a final ribbon of $(NH_4)_2MoS_4$ precursor in vertical (y-axis) direction is patterned for a desired length. This patterned structure is made in such a way that it overlaps with the other two structures at the desired point. Lastly, annealing is performed to crystallize the MoS_2 patterned structure. At the intersection of three ribbons, a vertical $MoS_2/WS_2/MoS_2$ heterostructure is formed.

To create lateral tri-layer heterostructures, a slightly different sequence of patterning steps is performed. First, $(NH_4)_2WS_4$ precursor ink is patterned in diagonal direction as a ribbon of a desired length. This is followed with the annealing process, to crystallize the WS_2 ribbon structure. Then, each of the two $(NH_4)_2MoS_4$ precursor patterns is made in such a way that it only touches the diagonal pattern of WS_2 on one side. This is the most challenging step in the patterning sequence for creating a lateral tri-layer heterostructure, as it is highly dependent on nanoscale precision capabilities of the instrument. The final step of annealing completes the process of lateral tri-layer $MoS_2/WS_2/MoS_2$ heterostructure formation.

Fig.S4 shows the schematics and representative optical images demonstrating the concept of creating $MoS_2/WS_2/MoS_2$ tri-layer heterostructures. The schematic representation of the $MoS_2/WS_2/MoS_2$ tri-layer vertical heterostructures is shown in Fig.S4a. Here it is easy to see that when additional layer of MoS_2 ribbon is formed on top of the WS_2/MoS_2 heterostructures, this effectively creates a tri-layer junction in the region. In this junction all three layers of materials are assembled on top of each other vertically. Optical image (Fig. S4b) shows a tri-layer vertical heterostructure of the $MoS_2/WS_2/MoS_2$. Similarly, the schematics of $MoS_2/WS_2/MoS_2$ lateral tri-layer heterostructure and an actual optical image of patterned $MoS_2/WS_2/MoS_2$ lateral tri-layer is shown in Fig. S4c and Fig. S4d, respectively.

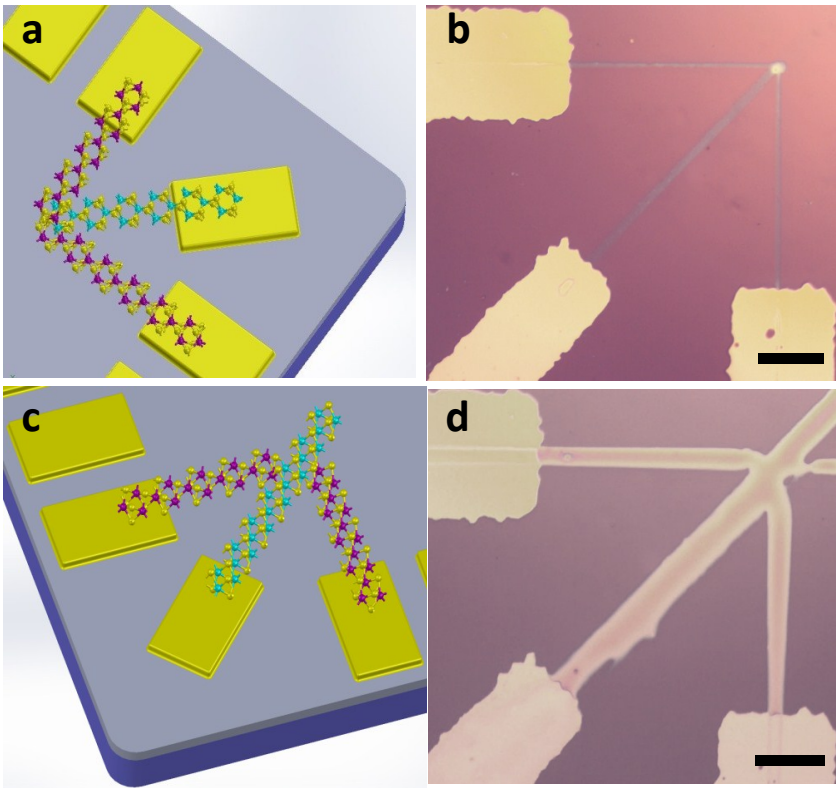

Fig. S4 The conceptual representation of $MoS_2/WS_2/MoS_2$ tri-layer heterostructures. a) the schematic representation of $MoS_2/WS_2/MoS_2$ tri-layer vertical heterostructure; b) the optical view of the

$MoS_2/WS_2/MoS_2$ tri-layer vertical heterostructures; c) the schematic representation of $MoS_2/WS_2/MoS_2$ tri-layer lateral heterostructure; d) the optical view of the $MoS_2/WS_2/MoS_2$ tri-layer lateral heterostructures. Yellow rectangular pads represent metal electrodes in a) and c), also seen in optical images in b) and d), (scale bars are ~ 100 μm).

5. Controlling of the MX_2 ribbon width and thickness.

In the direct writing of ribbons, the meniscus of water facilitates the continuous writing as tip moves along the surface and ink also self-diffuses in the lateral direction at the same time. With a relatively faster tip speed, we find that the process of ink lateral diffusion on the substrate can be controlled so that narrower ribbons are obtained. As suggested by the reviewer, we have added Table S1 where the relationship between the tip speed and the width of the MoS_2 ribbons is presented in detail. In these experiments (Table S1), as-prepared ink precursor (ammonium tetrathiomolybdate ($(NH_4)_2MoS_4$)) was used. Please note that with our present patterning tool the software capabilities allow only specific tip speed settings; those are indicated in the Table S1. The parameters in this table are also suitable for the process to control the width of WS_2 ribbons using as-prepared ammonium tetrathiotungstate ($(NH_4)_2WS_4$) ink precursor

Tip moving speed (μm/s)	Ribbon width (μm)
0.1	14~18
1	5~6
2	2.7~3.1
5	1.0~1.2

Table. S1 The relationship between the tip speed and the MoS_2 ribbon widths.

We have also demonstrated that the most convenient approach to determine the thicknesses of the resulting MoS_2 and WS_2 ribbons is to adjust precursor ink concentration. Table S2 was added to discuss in more detail the relationship between controlling parameters such as ink precursor (ammonium tetrathiomolybdate ($(NH_4)_2MoS_4$) concentration and the resulting thicknesses of MoS_2 ribbons. The tip moving speed in the measurements in Table S2 was set to 5 μm/s. Please note that because PTFE filtering is needed in our protocols for obtaining stable inks, hence the ink concentrations here are indicated as volume ratios of as-prepared ink to D.I. water. The obtained parameters shown in Table S2 are also suitable for the thickness control experiments for WS_2 patterned ribbons created with as-prepared ammonium tetrathiotungstate ($(NH_4)_2WS_4$) ink precursor.

Ink concentration (the volume ratio of as-prepared ink: D.I. Water)	Ribbon thickness (nm)
1:0	50~60
1:1	20~26
1:3	8~10
1:9	1.5~1.9

Table. S2 The relationship between the ink concentration and MoS_2 ribbon thicknesses.

6. HRTEM and XRD characterizations.

High-resolution transmission electron microscopy (HRTEM) was used for imaging the structure of MoS_2 material prepared by the thermal treatment of ammonium tetrathiomolybdate ($(NH_4)_2MoS_4$) as discussed in the manuscript. As shown in Fig.S5, the periodic atomic arrangement of the MoS_2 material structure at a selected location can be clearly observed. HRTEM characterization also demonstrates that heat-treatment of patterned $(NH_4)_2MoS_4$ structures with the presence of argon and hydrogen gas atmosphere would indeed lower the required MoS_2 crystallization temperature as described in the revised manuscript.

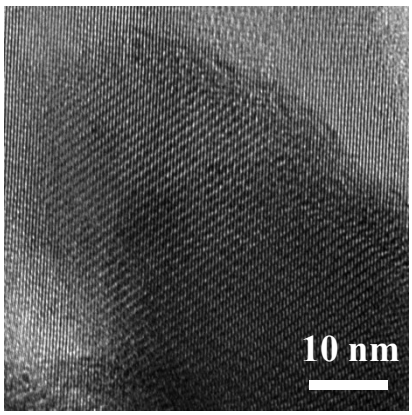

Fig. S5. Representative high-resolution TEM image depicting MoS_2 structure with well-defined atomic arrangement. Samples were prepared with same thermal treatment conditions as described in the manuscript Experimental section.

In addition, the presence of MoS_2 and WS_2 materials can be further demonstrated by the XRD (X-Ray diffraction) measurement. We found that the signal from as-prepared MX_2 patterned ribbons seemed too weak for detection using our XRD instrumentation set up (Rigaku XRD MiniFlex 600) which might be partly caused by an overall low coverage of the material on the substrate. Additional MX_2 samples were prepared for XRD measurement by the dip coating method with exact same inks and thermal treatment procedures as those used for ribbon preparations. In these samples the typical strong peak at approximately $2\theta \approx 14.3°$ for MoS_2 and WS_2 samples[4-6].

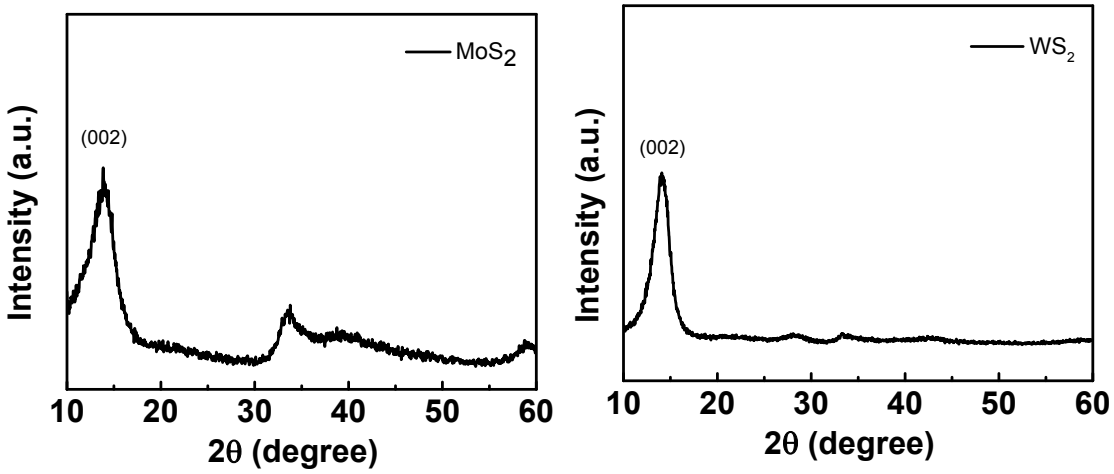

Fig. S6a) X-ray diffraction pattern of MoS_2 film; S6b) X-ray diffraction pattern of WS_2 film. The characteristic peaks at low angles at $2\theta \approx 14.3°$ are present for both materials.

1. I. Kuljanishvili, D. A. Dikin, S. Rozhok, S. Mayle and V. Chandrasekhar, *Small*, 2009, **5**, 2523-2527.
2. A. Urtizberea, M. Hirtz and H. Fuchs, Nanofabrication, 2015, 2, 43-53.
3. C. D. O'Connell, M. J. Higgins, D. Marusic, S. E. Moulton and G. G. Wallace, *Langmuir*, 2014, **30**, 2712-2721.
4. B. K. Miremadi and S. R. Morrison, *Journal of Applied Physics*, 1988, **63**, 4970-4974.
5. T. P. Nguyen, W. Sohn, J. H. Oh, H. W. Jang and S. Y. Kim, *The Journal of Physical Chemistry C*, 2016, **120**, 10078-10085.
6. H. S. S. Ramakrishna Matte, A. Gomathi, A. K. Manna, D. J. Late, R. Datta, S. K. Pati and C. N. R. Rao, *Angewandte Chemie International Edition*, 2010, **49**, 4059-4062.